## General Disclaimer

## One or more of the Following Statements may affect this Document

- This document has been reproduced from the best copy furnished by the organizational source. It is being released in the interest of making available as much information as possible.

- This document may contain data, which exceeds the sheet parameters. It was furnished in this condition by the organizational source and is the best copy available.

- This document may contain tone-on-tone or color graphs, charts and/or pictures, which have been reproduced in black and white.

- This document is paginated as submitted by the original source.

- Portions of this document are not fully legible due to the historical nature of some of the material. However, it is the best reproduction available from the original submission.

# LM CATHODE THRUSTER SYSTEM

## QUARTERLY PROGRESS REPORT NO.2, PHASE II

**4 OCTOBER 1969 through 4 JANUARY 1970**

**CONTRACT JPL 952131**

**by**

**J. HYMAN, JR , J.R. BAYLESS,**

**D.E. SCHNELKER and J.W. WARD,**

**15 JANUARY 1970**



HUGHES

HUGHES AIRCRAFT COMPANY

RESEARCH LABORATORIES

MALIBU, CALIFORNIA
90265

HUGHES RESEARCH LABORATORIES
Malibu, California

a division of hughes aircraft company

# LM CATHODE THRUSTER SYSTEM

Quarterly Progress Report No. 2, Phase II
4 October 1969 through 4 January 1970
Contract No. JPL 952131

J. Hyman, Jr., J. R. Bayless,
D. E. Schnelker, and J. W. Ward

15 January 1970

Performed for

Jet Propulsion Laboratory
California Institute of Technology

Sponsored by

National Aeronautics and Space Administration
Contract NAS 7-100 (Task Order #RD-26)

This report contains information prepared by the Hughes Research Laboratories under JPL subcontract. Its content is not necessarily endorsed by the Jet Propulsion Laboratory, California Institute of Technology, or the National Aeronautics and Space Administration.

## ABSTRACT

A 20 cm LM cathode thruster system is being developed for operation at beam currents $I_B$ = 0.5 A to 1.0 A and a beam voltage $V_B \lesssim 2$ kV. The thermal design and the thin-screen high-transparency ion-extraction system are similar to those of the 30 cm LM cathode thruster developed during the first phase of this contract. The discharge chamber configuration is derived from that of a 20 cm thruster with an externally cooled LM cathode, which had been optimized during the first phase for operation at a beam current $I_B \lesssim 600$ mA. The new thruster, which employs a thermally integrated LM cathode, has been assembled, and optimization-testing has begun. A liquid-mercury feed system is being assembled which consists of a high-voltage isolator, an electromagnetic pump, a liquid-mercury flowmeter, and a single-capillary flow impedance. Prototype models of each of these elements have demonstrated satisfactory operation under this contract. Thermal analysis confirms that the temperature of the thruster system remains within acceptable bounds for operation of an individual thruster, or for operation of an infinite planar cluster in which the separation between thruster centers is at least twice the thruster diameter.

# TABLE OF CONTENTS

# LIST OF ILLUSTRATIONS

# SECTION I

# INTRODUCTION

For detailed mission analysis or comparative evaluation of alternative thruster types, it is necessary to know the operating characteristics of an entire thruster system, including the subsystems for propellant feed, ion beam neutralization, and power conditioning. The development of each of these components for the LM cathode thruster system has now reached a stage where a laboratory-type thruster system (not involving flight-type power supplies) can be built based on existing technology. As a first step in the construction of this system, a thermally integrated 20 cm LM cathode thruster has been constructed and is now being tested for operation at beam currents $I_B$ = 0.5 to 1.0 A. A mercury feed system is also being assembled which consists of a hydrogen-bubble high-voltage isolator followed by an electromagnetic (EM) pump, a liquid-mercury flowmeter and a single-capillary flow impedance. These components combine to provide liquid mercury to an LM cathode which is thermally integrated with the 20 cm thruster. The feed system ultimately will be enclosed within the ground-screen shroud of the thruster and operated as part of a complete thruster system. The resulting LM cathode thruster system (designated the LMT-20-II system) requires only a mercury supply and the appropriate electrical power for its operation. No neutralizer cathode development is planned under this effort.

Programs for research and development of the LM cathode, the thruster, and various elements of the liquid-mercury feed system have been carried out as separately funded projects. Through coordinated guidance of the over-all program, however, these separate projects have produced the necessary devices and technology which will lead to the development of a reliable and useful laboratory-type thruster system.

The feasibility of LM cathode thruster life in excess of $10^4$ hours was demonstrated at Hughes Research Laboratories (HRL) under Contract NAS 3-6262; a 20 cm thruster equipped with a circular LM cathode was successfully tested for an accumulated 4,000 hours. No erosion of the molybdenum cathode structure was evident following this test, and there was no degradation of cathode performance. Development of high-temperature LM cathodes began at HRL under Contract NASW-1404 after it became apparent from thermal analysis that combining thrusters in peripheral or clustered arrays places a

constraint on the operation of any electron-bombardment ion thruster unless the temperature of the thruster shell can be allowed to exceed a value on the order of 200°C.

The demonstrated feasibility of system life in excess of $10^4$ hours, combined with a demonstrated capability for operation of a high-temperature LM cathode in an efficient thruster, prepared the way for the construction of a 30 cm thermally integrated thruster under the first phase of the current contract. This thruster has now demonstrated efficient performance at a specific impulse $I_{sp,\,eff}$ = 4,100 sec; a beam current $I_B$ = 1,400 mA is produced at a beam voltage $V_B$ = 2 kV with a source energy per ion $V_S$ = 270 eV/ion* at a mass utilization efficiency $\eta_m$ = 90%. At this power level, the thermally integrated LM cathode achieves an equilibrium body temperature $T_K$ = 200°C; it rejects the heat from the discharge along a tapered aluminum endplate to the outer thruster shell, from which the heat is radiated to the walls of the vacuum chamber.

In a related contract effort (Contract NAS 7-539), the design of liquid-mercury feed systems was explored in detail. A number of unique components were built so that their operating characteristics could be established and the various systems which were considered could be properly evaluated. Two of these components, an EM pump and a high-voltage isolator, have since been incorporated into a breadboard flow system which was operated under the first phase of the current contract for a final demonstration of the proper operation of each of the components and of the mutual compatibility of all of the components of the system. The feed system consisted of (1) a gas-pressurized positive-expulsion mercury reservoir, (2) the liquid-mercury high-voltage isolator, (3) the EM pump, (4) a single-capillary flow impedance, and (5) a high-temperature LM cathode which was thermally integrated with the 30 cm electron-bombardment thruster. Successful operation of the 30 cm LM cathode thruster with the bread-board liquid-mercury feed system led to the present development of the LMT-20-II thruster system.

---

*$V_S$, the total source energy per ion, is the discharge energy per ion, because no heater, vaporizer, or keeper power is required with the LM cathode.

## SECTION II

## LM CATHODE THRUSTER SYSTEM

The thermally integrated 20 cm LM cathode thruster has been assembled, and optimization-testing has begun. The thruster body is constructed mainly of aluminum except for the ion-optics, which are made of molybdenum. The over-all mass of this thruster is about 4 kg, including the mass of the heat shields and the LM cathode, but not including the mass of the feed system or the ground-screen shroud. Measured values for the masses of all system components are given in Table I. Figure 1 shows the new 20 cm thruster (designated the LMT-20-II thruster*) mounted on the vacuum chamber endplate. For initial thruster operation, a high-temperature LM cathode with a piston-driven liquid mercury feed system (not including an electromagnetic pump, high-voltage isolator, or liquid mercury flowmeter) is being used. By this expedient, separate development of the complete feed system can proceed simultaneously with optimization of the new thruster prior to integration of all system components.

---

*The total thruster system has been designated the LMT-20-II thruster system, etc. The experimental 20 cm thruster (which was optimized for operation at lower beam currents during the first phase of this contract) is designated the LMT-20-I thruster, and the 30 cm thruster is designated the LMT-30-I thruster.

# TABLE I

## Component Masses of the LMT-20-II Thruster System

| Component | Part No. | Quantity per Assembly | Weight of Assembly, kg |
|---|---|---|---|
| Thruster | | | |
| Thruster Shell Assembly | 839924 | 1 | 0.499 |
| Band, Anode Feedthrough | 839925 | 1 | 0.046 |
| Anode, Upstream | 839926 | 1 | 0.132 |
| Anode, Downstream | 839927 | 1 | 0.076 |
| Outer Anode Connector | 839928 | 1 | 0.087 |
| Ceramic Spacer | 839929 | 8 | 0.012 |
| Accel. Electrode | 839930 | 1 | 0.444 |
| Screen Electrode | 839946 | 1 | 0.155 |
| Stud | 839931 | 4 | 0.022 |
| Shield Insulator | 839932 | 8 | 0.014 |
| Bracket, Insulator, Center | 839933 | 4 | 0.039 |
| Support, Insulator, Accel. | 839934 | 4 | 0.062 |
| Support, Magnet, Upstream | 839937 | 1 | 0.125 |
| Splice Plate Assembly | 839938 | 1 | 0.005 |
| Pole Piece, Outer, Upstream | 839940 | 2 | 0.141 |
| Pole Piece, Inner, Upstream | 839941 | 2 | 0.044 |
| Pole Piece, Upstream Cover | 839942 | 1 | 0.057 |
| Screen Pole Piece | 839947 | 1 | 0.349 |
| Magnet With Windings | 839948 | 8 | 0.884 |
| Nut & Screw-Mtg. Anode Sink | 1024015 | 16 | 0.066 |
| Ceramic Insulator, Feedthrough | 1024016 | 8 | 0.088 |
| Feedthrough, Anode | 1024017 | 8 | 0.048 |
| Screw, Shouldered | 1024018 | 8 | 0.003 |
| Removable Endplate | 1024128 | 1 | 0.183 |
| LM Cathode K-54 | | 1 | 0.131 |
| Heat Shields | | 10 | 0.309 |
| Total | | | 4.021 |
| Feed System | | | |
| Plate, Feed System Support | 1024127 | 1 | 0.036 |
| Mount, Flowmeter | 1024129 | 1 | 0.002 |
| Mount - EM Pump | 1024130 | 1 | 0.005 |
| Retaining Nut, Isolator Connector | 1029132 | 1 | 0.005 |
| Connector Isolator | 1029134 | 2 | 0.001 |
| Hydrogen Reservoir | 1024145 | 1 | 0.218 |
| Isolator | | 1 | 0.089 |
| EM Pump | | 1 | 0.301 |
| Flowmeter | | 1 | 0.098* |
| "Swagelok" Couplings | | 6 | 0.112 |
| Plate, Feed System | 1024059 | 1 | 0.111 |
| Capillary Impedance | | 5m | 0.040 |
| Total | | | 1.008 |
| Ground-Screen Shroud | | | |
| Accel. Extension | 1024019 | 1 | 0.094* |
| Ground Screen, Center | 1024020 | 1 | 0.240* |
| Ground Screen, Optics Insulator | 1024021 | 1 | 0.130* |
| Ground Screen, Neutralizer Cover | 1024022 | 1 | 0.013 |
| Ground Screen, End Cover | 1024024 | 1 | 0.096 |
| Ground Screen, Feed System | 1024114 | 1 | 0.197 |
| Stud | 839931 | 8 | 0.050 |
| Shield Insulator | 839932 | 16 | 0.028 |
| Ceramic Spacer | 839929 | 16 | 0.024 |
| Support, Insulator, Center | 839935 | 4 | 0.012 |
| Support, Insulator, Upstream | 839936 | 4 | 0.024 |
| Total | | | 0.908 |
| Total Weight of Assembly | | | 5.947 |

*Masses marked by an asterisk have not yet been measured and their values are estimated.

M 6936

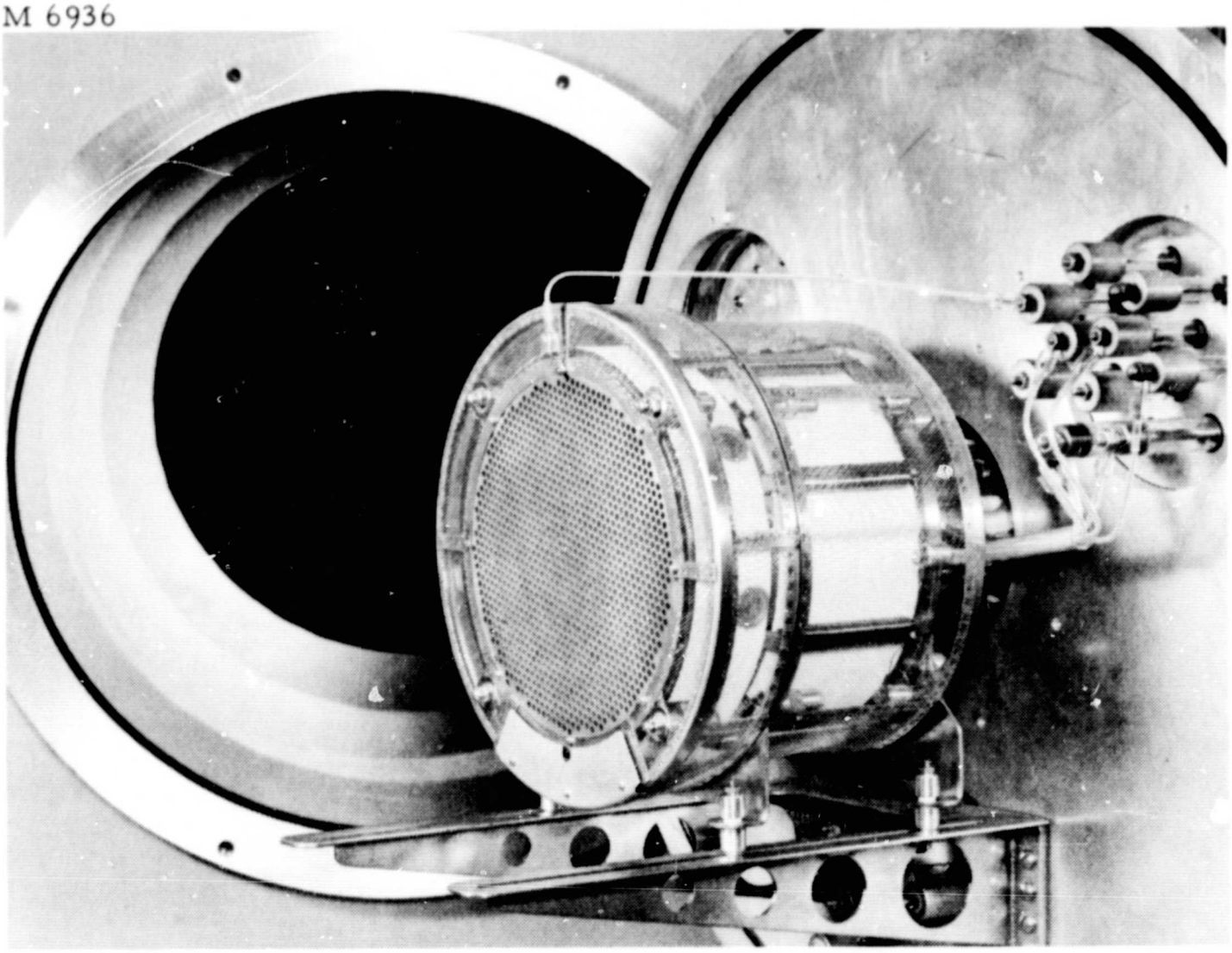

Fig. 1. The LMT-20-II thruster is shown mounted on the vacuum chamber endplate.

# SECTION III

# THERMAL ANALYSIS

Detailed thermal analysis is required to establish accurate quantitative criteria for the design of a lightweight thermally integrated LM cathode thruster. The first detailed analysis of an electron-bombardment thruster was undertaken at HRL under Contract JPL 952129, in which a thermal simulation of the ion-extraction system was carried out. Because of the limitations of that program, the simulation did not include the discharge chamber.

A complete thermal simulation of the thermally integrated LM cathode thruster is being undertaken as part of the present effort. This work involves the following tasks: (1) carry out a detailed thermal simulation of the discharge chamber, (2) combine the simulations of the discharge chamber and ion-extraction system, (3) compare the predictions of the thermal simulation with temperatures measured experimentally with the LMT-30-I thruster to improve the accuracy of thermal simulation, (4) use the proven simulation to analyze the thermal characteristics and improve the design of the LMT-20-II thermally integrated LM cathode thruster, and (5) correlate the calculated thermal data with temperatures measured experimentally with the LMT-20-II thruster in order to evaluate the thermal design.

Computer program TAS-1B, which is being employed to thermally simulate the discharge chamber, is a digital computer program which solves for the steady-state temperature distribution in a lumped parameter network of temperature points (nodes) and heat flow paths (resistors). The inputs to TAS-1B which are required to model a device are the heat losses, nodal areas, radiant emissivities, radiation view factors, and thermal conductances. The heat inputs are determined for the most part from physical considerations which are based on an extension of a theory of discharge mechanisms which was developed by W. Knauer at HRL.[1] General relationships have been determined to facilitate calculation of the remaining quantities for a discharge-chamber model comprising 28 nodes. The generality of these relationships expedites thermal analysis over an entire range of geometrical variations of the thruster configuration. A small computer program has been written to automate this calculation. Figure 2 illustrates the configuration of nodes which was described in Quarterly Progress Report No. 1 (Phase II).

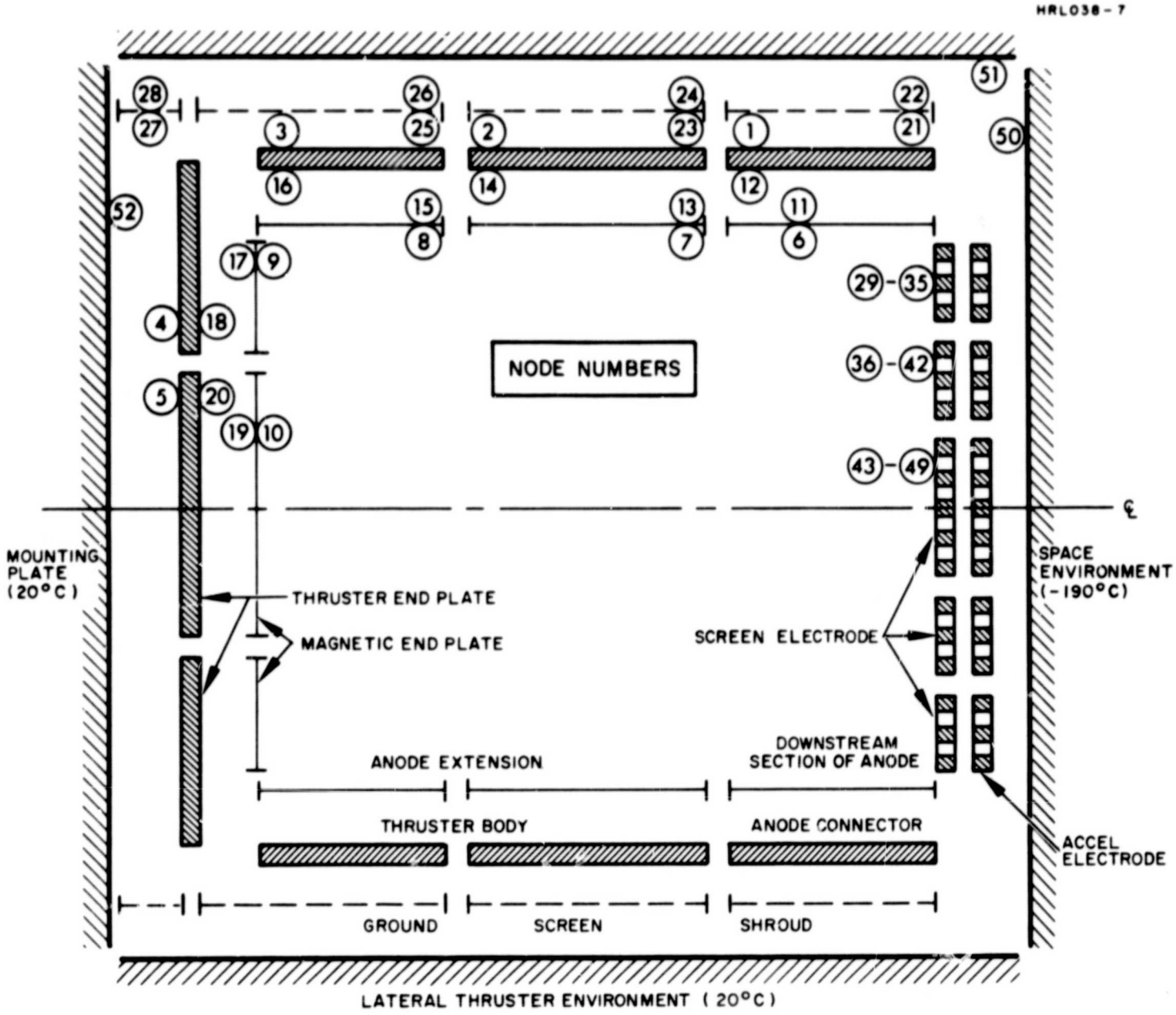


Fig. 2. Configuration of nodes used to simulate the thermal characteristics of an LM cathode thruster. The numbering of nodes is indicated in the upper half of the schematic.

The thermal profile of the LMT-30-I thruster has been calculated and shown to agree with the measured profile, thus demonstrating the efficacy of the thermal simulation. Subsequently the thermal profile of the LMT-20-II thruster has been determined for a variety of environmental conditions on the basis of this proven analytical approach.

## A. DISCHARGE CHAMBER HEAT DISTRIBUTION

A physical theory which postulates a discharge mechanism for the electron-bombardment thruster has been developed by Knauer for determining the limits of power efficiency of these thrusters.[1] With only slight modifications, the same physical considerations were employed in Quarterly Progress Report No. 1 (Phase II) of this contract to determine the distribution of heat inputs to an LM cathode thruster which arise from discharge chamber losses. In the following discussion, a more complete analysis is presented which includes (among other things) the effects due to the work-function potentials of the various electrode surfaces.

The same general assumptions as those used by Knauer are assumed to apply to the LM cathode thruster:

1. The plasma is uniformly distributed within the discharge chamber.

2. The plasma electrons in the discharge chamber possess a Maxwellian energy distribution with a temperature $T_p$ which is constant throughout the chamber.

3. The plasma potential in the discharge chamber is uniform at a value $\Delta V_A$ above the node potential $V_A$, except for positive potential barriers and sheaths near walls.

4. The ion extraction screen is at cathode potential and permits passage of a fraction $\alpha$ of the arriving ions. The remaining fraction $(1 - \alpha)$ is neutralized upon impact, and re-enters the discharge traveling in the upstream direction.

5. The endplate of the discharge chamber is held at cathode potential and all impacting ions recombine and come off as neutrals.

6. Ions are prevented from reaching the anode. This assumption is based on the plasma-probe measurements (by Eckhardt, et al.,[2] with an LM cathode thruster and by Knauer, et al.,[3] with both hollow- and oxide-cathode thrusters) which indicate the existence of a small positive potential ridge near the anode which prevents the impingement of ions which originate at the center of the discharge chamber.

For the LM cathode, the following specific assumptions are made:

7. A uniform plasma exists within the cathode-cup pole piece which has a potential $V_C$ relative to the cathode and a Maxwellian electron energy distribution of temperature $T_C$.

8. Energy is delivered to the cathode-cup plasma by electrons which accelerate from the cathode into this plasma. This energy goes into (1) releasing electrons from the cathode wall, (2) heating of the cathode, (3) thermal energy of "primary" electrons which leave the cathode cup, and (4) heating of the cathode cup.

Employing these assumptions, the minimum total source energy per beam ion $V_S|_{min}$ for an electron-bombardment thruster has been shown by Knauer to be equal to

$$V_S|_{min} = \frac{\beta\,\delta}{\eta_m}\,V_A + \left(\frac{\delta}{\eta_m} - 1\right)\,V_A. \qquad (1)$$

The terms introduced in this equation are defined below:

The quantity

$$\beta = \frac{\text{minimum number of primary electrons}}{\text{ionization}} = \frac{\text{energy consumption per ionization}}{\text{maximum energy available from "primary" electron}}$$

or

$$\beta = \frac{eV_i + e\Delta V_A + \frac{3}{2}kT_p + \frac{1}{\nu_i}\sum_n eV_n\,\overline{\nu}_n}{e(V_A - V_C) + \frac{3}{2}kT_C - \frac{3}{2}kT_p}$$

where $V_i$ is the propellant ionization potential (for mercury $V_i$ = 10.4 V), $\nu_i$ is the ionization frequency averaged over the electron energy distribution, $\nu_n$ is the averaged excitation frequency due to collisions of atomic energy level n, $V_n$ is the potential energy of level n, and k is the Boltzmann constant. The quantity $\eta_m$ is the mass utilization efficiency and

$$\delta = \frac{\text{number of ionizations}}{\text{atom}} = \eta_m\left(\frac{2}{\alpha} - 1\right).$$

As before, $\alpha$ is the transparency of the ion extraction system.

In practice, the measured value of source energy per ion $V_S$ will exceed the minimum value to some extent as a result of less-than-optimum containment of "primary" electrons. Incomplete containment causes the average "primary" electron to arrive at the anode with an extra energy $\Delta E$ above the minimum possible average energy of $3/2\ kT_p$. Knauer's theory can be modified to include these additional losses by subtracting $\Delta E$ from the denominator in the expression for $\beta$ and including it in the calculation of the term $1/\nu_i \sum_n eV_n \nu_n$ appearing in the numerator. Thus, for an LM cathode thruster which has not yet been optimized to the fullest extent, a new value $\beta'$ can be written as

$$\beta' \equiv \frac{eV_i + e\Delta V_A + \frac{3}{2} kT_p + \frac{1}{\overline{\nu}_i (\Delta E)} \sum_n eV_n \overline{\nu}_n (\Delta E)}{e(V_A - V_C) + \frac{3}{2} kT_C - \frac{3}{2} kT_p - \Delta E}$$

For experimentally measured values of the source energy per ion $V_S$, eq. (1) can now be modified as follows:

$$V_S = \frac{\beta'\delta}{\eta_m} V_A + \left(\frac{\delta}{\eta_m} - 1\right) V_A. \qquad (2)$$

Equation (2) is then used to evaluate the quantity $\beta'$, from which the value of the quantity $\Delta E$ can be determined.

The distribution of heat inputs to the body of an LM cathode thruster can be evaluated in terms of the quantities defined above. The heat per beam ion which is lost to the cathode is given by

$$E_K = \frac{\beta'\delta}{\eta_m} V_{K,th}$$

where $V_{K,th}$ is the specific thermal loading of the cathode (see Section IV-C). The relationship for the heat per beam ion which is lost to the cathode cup is

$$E_C = \frac{\beta'\delta}{\eta_m} \left(V_C - \frac{3}{2} \frac{kT_C}{e} - V_{K,th} - \phi_K\right).$$

where $V_C$ represents the total kinetic energy acquired by the electrons which accelerate from the cathode surface into the cathode-cup plasma. Of the three subtracted quantities, $3/2\ k/e\ T_C$ represents the average thermal energy carried away by electrons leaving the plasma of the cathode cup, $V_{K,th}$ represents the heating of the cathode itself, and $\phi_K$ is the work function potential which is required to liberate each electron from the cathode surface. Of the total kinetic energy, only the amount which remains after the three subtractions results in heating of the cathode cup.

Ions which reach thruster surfaces which are at cathode potential gain kinetic energy in falling through the potential drop. The heat per beam for $E_W$ which is lost to these walls is equal to the sum of the incident kinetic energy plus the difference between the energy of recombination $V_i$ and the work-function potential $\phi_k$ which is required to extract an electron from these surfaces.

$$E_W = \left( \frac{\delta}{\eta_m} - 1 \right) \left( (V_A + \Delta V_A) + (V_i - \phi_K) \right).$$

The heat per beam ion $E_A$ which is carried to the anode by collected electrons is given by

$$E_A = \frac{\beta' \delta}{\eta_m} \frac{\Delta E}{e} + \left( \frac{\beta' \delta}{\eta_m} + \frac{\delta}{\eta_m} \right) \left( \frac{3}{2} \frac{kT_p}{e} + \phi_A \right).$$

The energy per beam ion $E_\nu$ which goes into excitation processes is given by the relationship

where

$$E_\nu = \frac{\delta}{n_m} E'_\nu$$

$$E'_\nu = \frac{1}{\bar{\nu}_i} \sum_n \bar{\nu}_n V_n.$$

(For the present analysis an approximate value $E'_\nu = 10$ eV is used.)

The inputs listed above represent thermal losses which are incurred in the process of generating the ion beam. The discharge power supply also provides the creation energy $E_i$ for each ion entering the beam. This can be expressed as the potential energy of the ion relative to the potential of the anode electrode*

$$E_i = \Delta V + (V_i - \phi_A) \quad .$$

The sum of all the energy expenditures per beam ion which are listed above is equal to the total source energy per beam ion $V_S$.

From experimentally measured operating parameters, the heat losses to an LM cathode thruster can now be determined. Using these as inputs to computer program TAS-1B, the temperature distribution for the LMT-30-I thruster is calculated below and compared with the measured distribution to demonstrate the efficacy of the analytical model.

Typical operating conditions for the LMT-30-I thruster are:

| | | |
|---|---|---|
| Beam current | $I_B$ | = 1.09 A |
| Mercury flow rate equivalent | $I_a$ | = 1.32 A |
| Discharge current | $I_K$ | = 7 A |
| Discharge voltage | $V_A$ | = 45 V |
| Source energy per ion | $V_S$ | = 289 eV/ion |
| Mass utilization efficiency | $\eta_m$ | = 82.5% |
| Special thermal load | $V_{K,th}$ | = 4 W/A. |

Values for the electron temperatures and floating potentials of the discharge plasma are obtained from the results of Knauer, et al.[3] Although these data were generated with a hollow-cathode thruster, it is

*For consistency in this analysis, the potential energy of both the beam ion and its associated secondary electron (generated as the other part of the ion pair) have been referenced to the Fermi level of the bound electrons within the anode material.

thought that they are more representative of the values to be found in the present LM cathode thrusters than are the existing data which were measured with an LM cathode thruster prior to optimization of that thruster under the current contract. From the operating conditions listed above, values of the distribution of heat inputs to the LMT-30-I thruster are calculated as follows (refer to Fig. 3):

- Power to cathode (input to node 5) $P_K = I_K I_B = 24.2$ W
- Power to cathode cup (half is assumed to be radiated to node 10 and the remaining half is radiated uniformly to all other nodes which are inside the discharge chamber) $P_C = E_C I_B = 21.2$ W
- Power to cathode-potential walls (deposited uniformly in nodes 9, 10, 35, 42, and 49) $P_W = E_W I_B = 51.1$ W
- Power to anode (67% of $P_A$ is delivered to the front third of the anode, with the remainder distributed uniformly over the rest of the anode surface) $P_A = E_A I_B = 187$ W
- Power going into excitations (subsequently distributed uniformly as heat to all nodes which are inside the discharge chamber) $P_\nu = E_\nu I_B = 21$ W

The total power which is delivered to the anode was distributed to result in agreement with the experimental temperature measurements. In addition, the following heat losses are included which are generated outside the discharge chamber:

Power to the accel electrode (delivered to nodes 41 and 48) $P_{Ac} = 12.8$ W

Power dissipated in the magnets (half goes into nodes 1, 2, and 3 and half into nodes 21, 23, 25, and 51) $P_M = 12$ W

The values of the radiation emissivities are representative of the surfaces of the various materials employed in fabricating the thruster.[4] Multiple heat shields are included into this analysis by an effective emissivity $\epsilon_e$, as discussed[5] in Quarterly Progress Report No. 1 (Phase II). The emissivities, heat inputs, and resultant temperature profile for the LMT-30-I thruster are illustrated in Fig. 3. These results agree with the measured temperature profile described earlier. Those measurements indicated that all external thruster

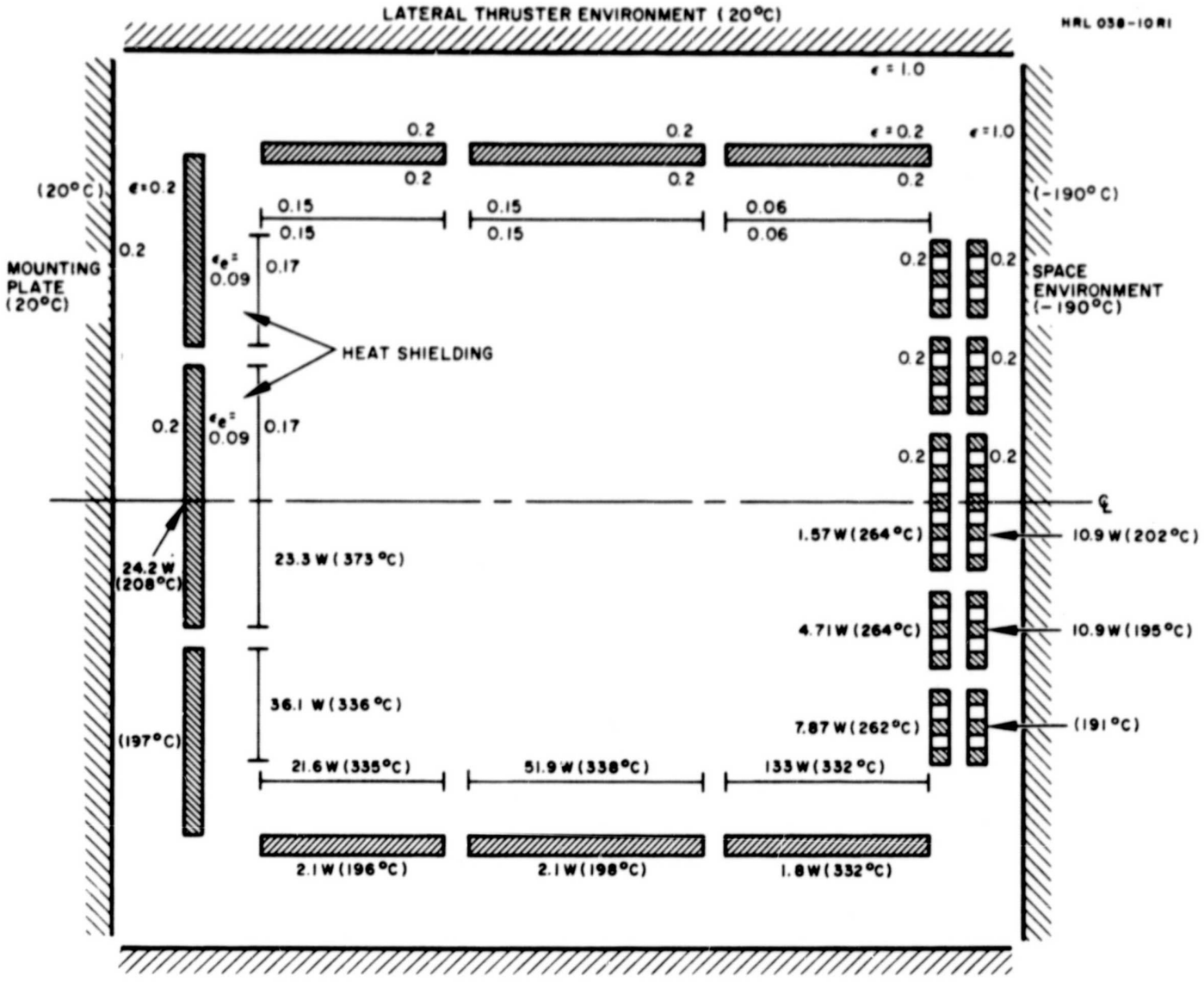


Fig. 3. Thermal model of the LMT-30-I thruster operating at a beam current $I_B$ = 1.09 A. The emissivities and temperatures of fixed temperature walls are noted in the upper half of the schematic. The heat inputs and resultant temperature distribution are indicated in the lower portion of the diagram.

surfaces operated at less than 200°C, except for the external anode connector which reached a temperature of 281°C. The thin stainless-steel anode extension achieved a uniform temperature which was within 2°C of the downstream section of the anode. The good agreement between the experimental and analytical results with the LMT-30-I thruster indicates the usefulness of the analytical approach for thermal design of LM cathode thrusters in general.

## B. THERMAL DESIGN

The proven thermal analysis has been employed in the design of the LMT-20-II thruster in an effort to predetermine its thermal operating characteristics. In addition to the study of the characteristics of a single thruster which radiates to space, emphasis has also been focused on the effect of assembling groups of thrusters in clustered arrays.

For these analyses, the operating conditions of the LMT-20-II thruster are taken to be

| | | |
|---|---|---|
| Beam current | $I_B$ | = 1 A |
| Mercury flow rate equivalent | $I_a$ | = 1.18 A |
| Discharge current | $I_K$ | = 7 A |
| Discharge voltage | $V_A$ | = 40 V |
| Source energy per ion | $V_S$ | = 280 eV/ion |
| Mass utilization efficiency | $\eta_m$ | = 85% |
| Specific thermal load | $V_{K,th}$ | = 4 W/A* |

*The specific thermal load for the LM cathode $V_{K,th}$ is treated as a constant in the present calculations. For more precise results the dependence on temperature should be included and a self-consistent solution must be found. The temperature dependence of the specific thermal loading [$V_{K,th}$ ($T_K$)] for LM cathode K-51 is given in Fig. 11, Section IV-C.

The outer surfaces of the thruster body are covered with high emissivity ($\epsilon = 0.85$) paint, and the values of the remaining emissivities are representative of the various materials employed in fabricating the thruster surfaces.[4] The emissivity of the upstream side of the thruster was set to zero in order to represent thermal isolation of the feed system mounted adjacent to that surface. Eleven heat shields, consisting of 6061 aluminum foil, cover both the inside surface of the thruster endplate and the upstream two-thirds of the anode extension. The heat shielding which covers the anode extension is visible in the photograph of the LMT-20-II thruster, which is shown in Fig. 4.

The emissivities, heat inputs, temperatures of fixed temperature walls, and resultant temperature profile are illustrated in Fig. 5 for a single thruster radiating to space. For this case the cathode attains a temperature of 121°C, which is well within acceptable limits of operation.

The same thruster conditions have been employed to study the effects of combining many thrusters in a clustered planar array. Each thruster was assumed to be surrounded on all sides by a large number of identical thrusters, so that heat could be radiated only in the direction of the ion beam. The situation was analyzed by setting the emissivity of the lateral boundary of the thruster environment equal to zero (a reflecting boundary), in order to simulate the case of a central thruster surrounded by a set of identical thrusters which are separated by twice the distance of the reflecting boundary. The radius of this lateral boundary $R_e$ was varied between 1.5 and 3 times the thruster radius R, in order to vary the view factor between the thruster side walls and the space environment. Figure 6 illustrates how the cathode temperature depends on the ratio $R_e/R$. At a beam current of 1 A, a self-consistent solution for operation of the LMT-20-II thruster with LM cathode K-51 (i.e., $V_{K,th} = 4$ W/A at $T_K = 155$°C) is achieved at a value $R_e/R = 2.6$, which occurs when the spacing between thrusters is 2.6 times the thruster diameter. Closer spacings can be accommodated by use of an alternative LM cathode which exhibits a low value of specific thermal loading at higher temperature. The specific thermal loading of LM cathode K-25-V, for example, reaches the value of specific thermal loading assumed for this analysis at a cathode body temperature $T_K = 205$°C. With this cathode, the required separation between thruster centers is reduced to 2.03 times the thruster diameter. For still closer spacings, additional means for heat dissipation are required. This can be provided by allowing heat conduction between the thruster and the spacecraft (for the present configuration, no such mechanism for such heat transfer is permitted) or by using an addition radiator which can be connected to the thruster cathode by a heat pipe or other means.

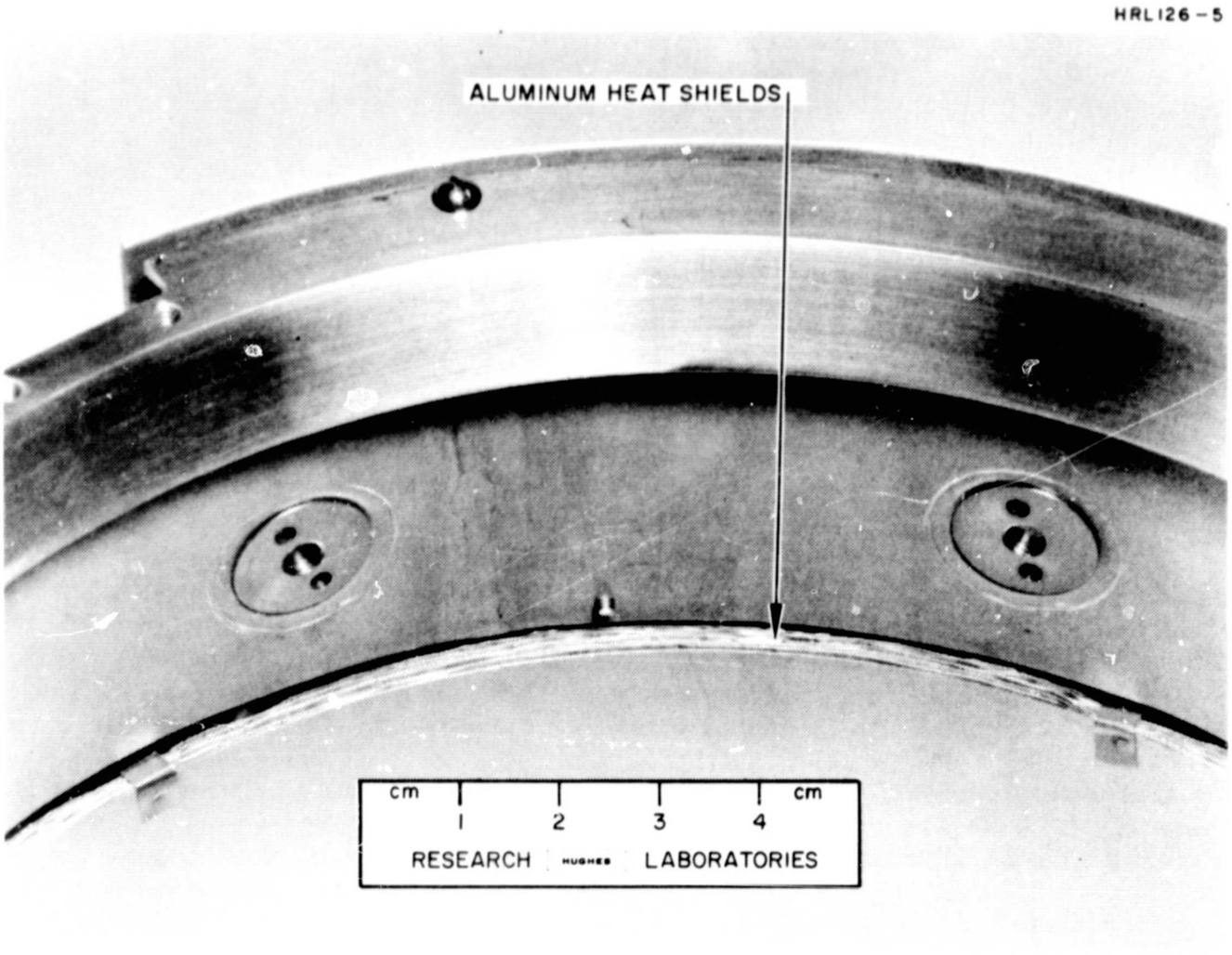


Fig. 4. The LMT-20-II thruster showing the heat shielding which covers the anode extension.

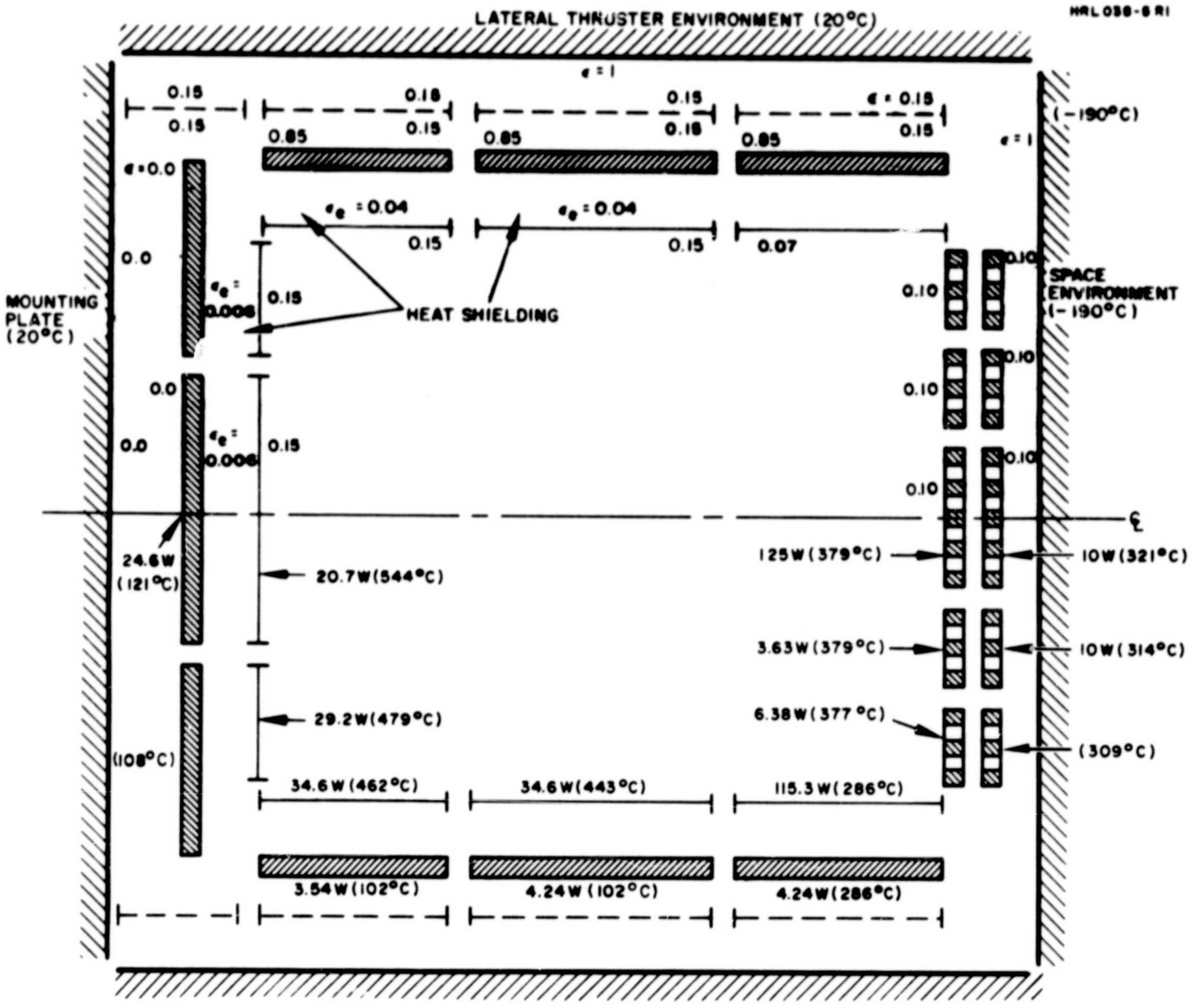


Fig. 5. Thermal model of the LMT-20-II thruster operating at a beam current $I_B$ = 1 A. The emissivities and temperatures of the fixed-temperature walls are noted in the upper half of the schematic. The heat inputs and resultant temperature distribution are indicated in the lower portion of the diagram.

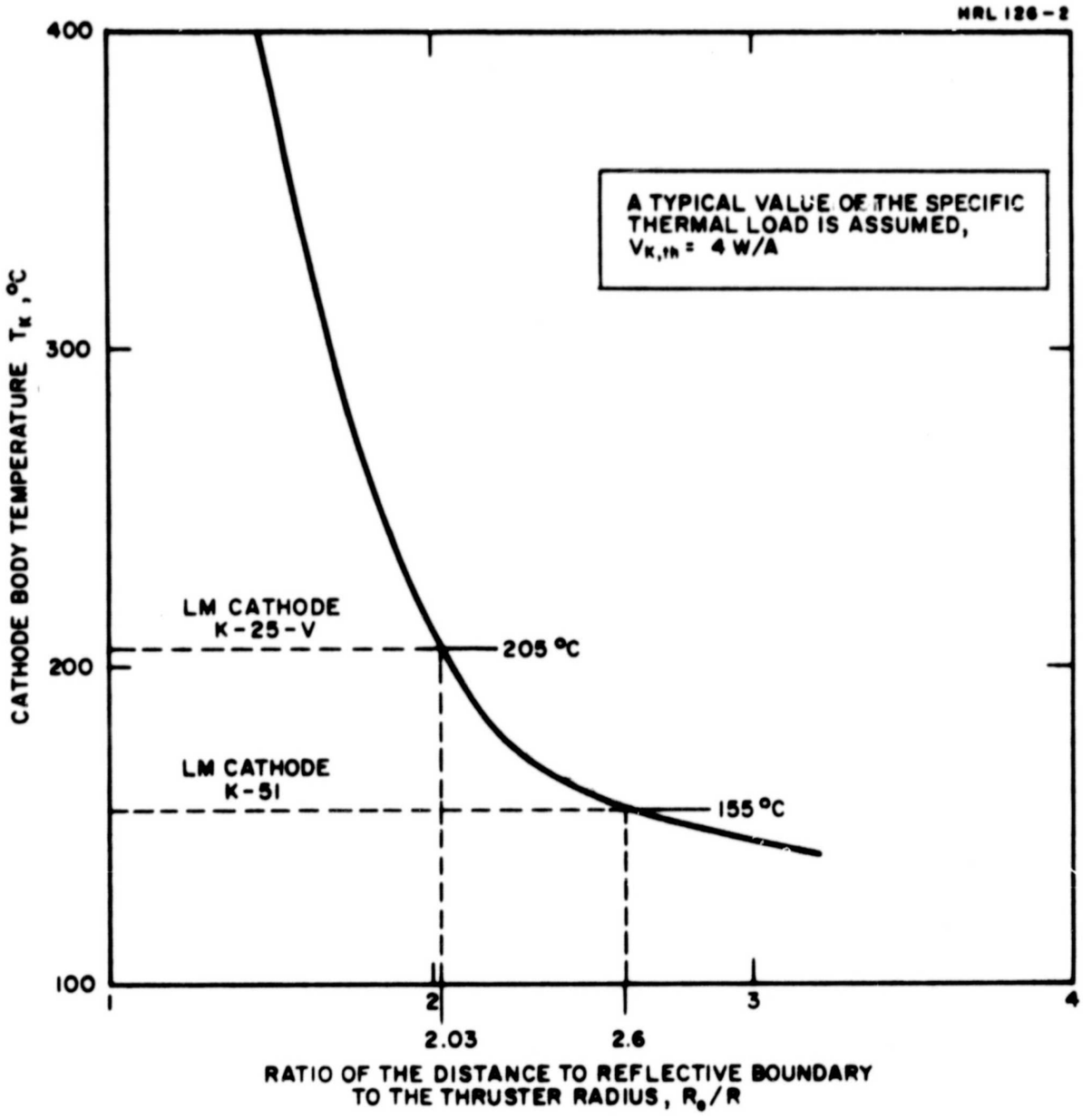


Fig. 6. Dependence of cathode temperature (T/K) on spacing between thrusters in an infinite array. The thruster radius is R, and $R_e$ is effectively equal to one-half the distance between thruster centers.

# SECTION IV

# COMPONENT DEVELOPMENT

## A. OPTIMIZATION OF THE LMT-20-I THRUSTER

The LMT-20-I thruster was optimized for operation at low beam currents during the first phase of the current contract. Under the current phase, this thruster has undergone a series of modifications in which the configuration was changed to resemble that of the new LMT-20-II thruster. The modifications were carried out in stages in an attempt to preserve the previously existing high efficiency of thruster performance while extending operation to beam currents in the range $I_B$ = 0.5 to 1.0 A.

In the first stage of modification, the LMT-20-I thruster was equipped with a thin-screen (0.078 cm thick) high-transparency (71%) ion extraction system which is similar to that employed with the LMT-20-II thruster. After a series of nine variations in discharge-chamber geometry, the best over-all performance of the series was achieved with the configuration shown in Fig. 7. The cathode-cup pole piece is larger than any used previously with this thruster; it is 5.08 cm long, with an outside diameter of 6.7 cm and a wall thickness of 0.076 cm. A total of 12 holes (each 1.19 cm diameter) penetrate the side walls of the pole piece. The holes are covered with a 20 wire/cm stainless steel mesh which is 50% transparent to neutral particle flux. A baffle with a conical edge was used to permit continuous variation of the width of the baffle gap with baffle position d.

As shown in Fig. 8, the discharge-chamber performance obtained with this configuration was fairly uniform throughout the range of beam current tested (700 mA < $I_B$ < 940 mA; no observations were taken beyond this range). This level of performance was judged to be sufficiently high to warrant proceeding to the next stage in modification of the LMT-20-I thruster toward the configuration of the new LMT-20-II thruster.

In the second stage of modification, the six bar electromagnets employed originally in the LMT-20-I were replaced by an alternative set which better simulates the configuration of the eight bar electromagnets which are used in the LMT-20-II thruster. The sum of the cross-sectional areas of the six replacement magnets is equal to that of the eight electromagnets of the new thruster, and the windings extend

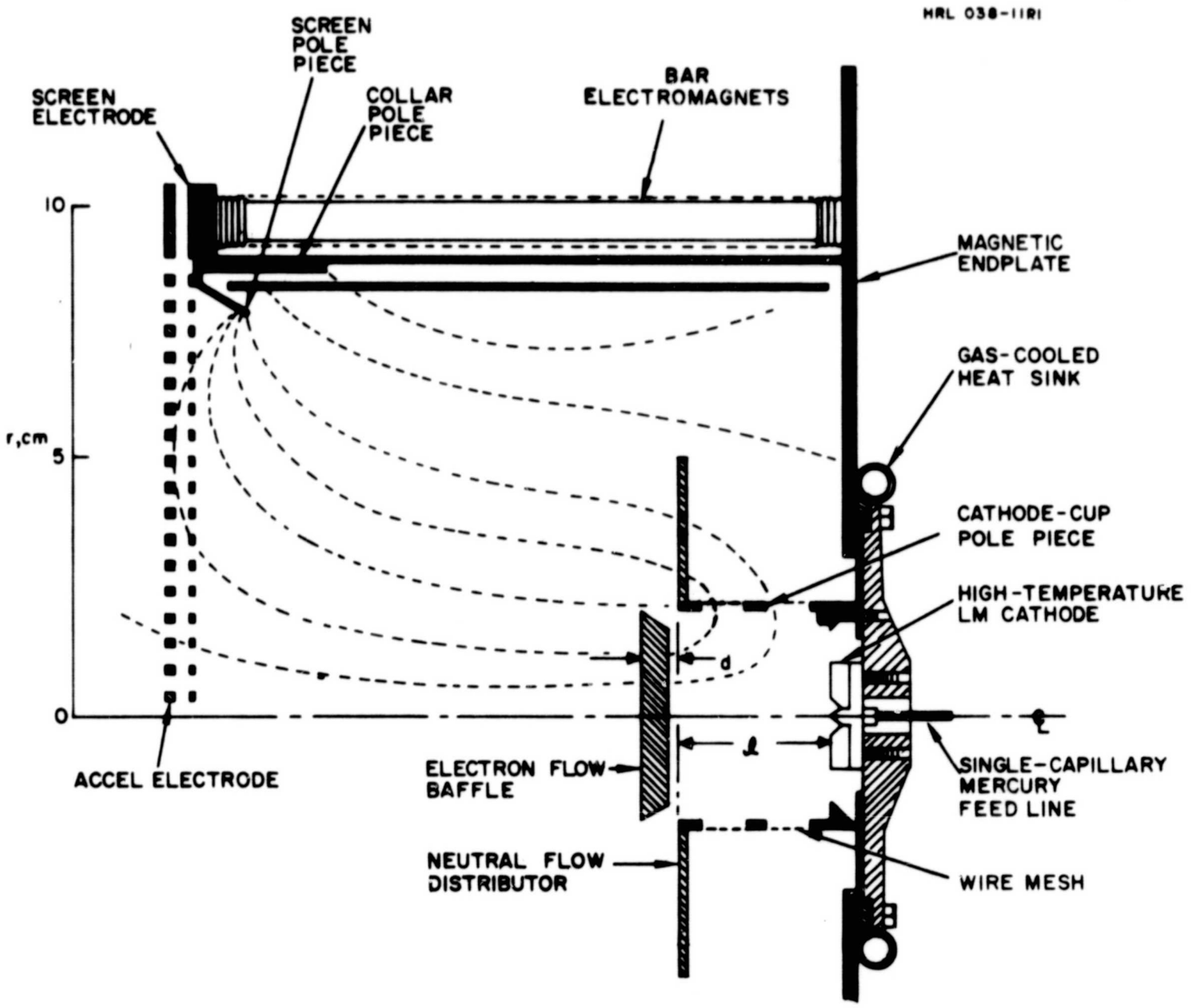


Fig. 7. The LMT-20-I thruster in its ninth variation.

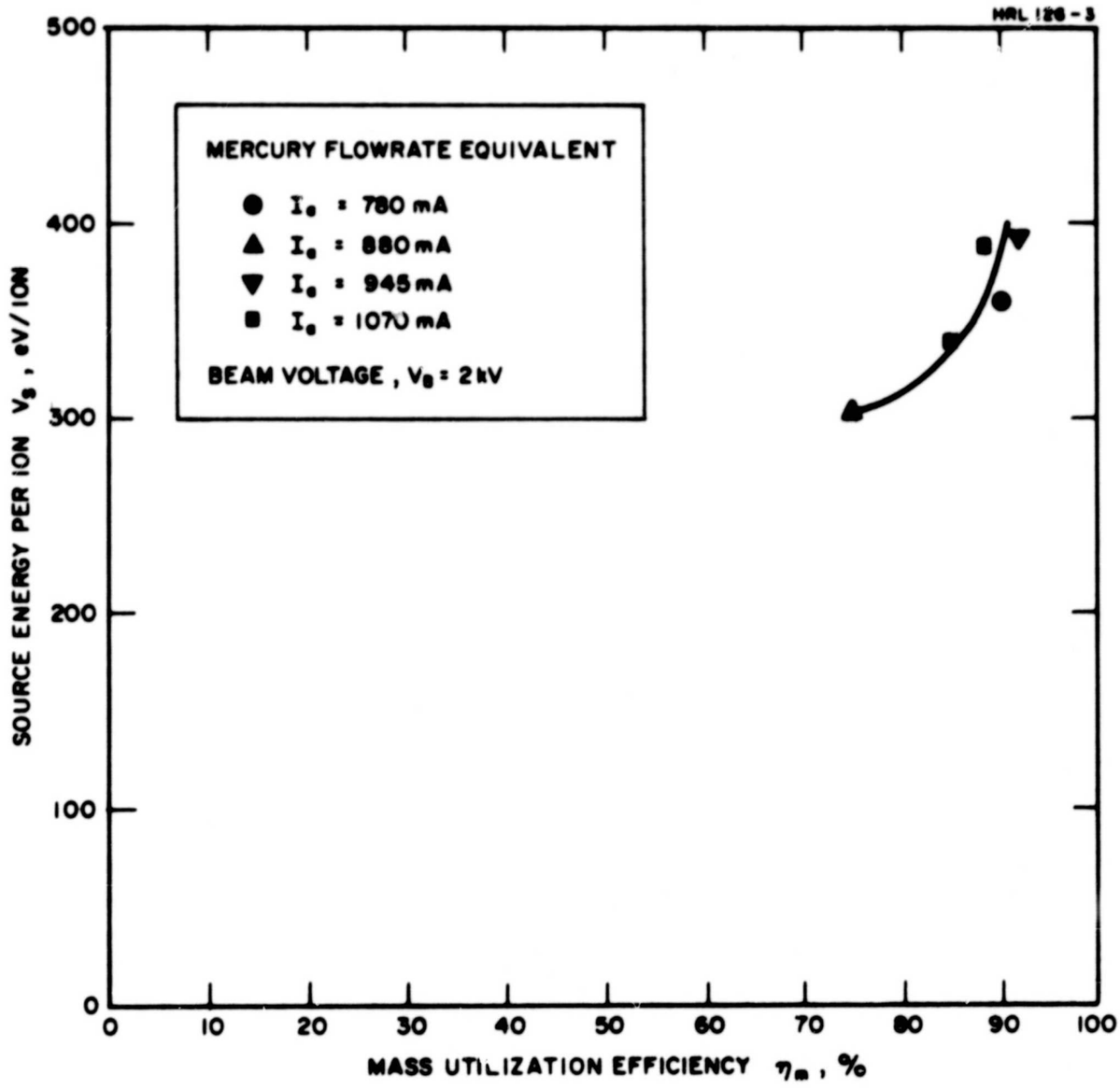


Fig. 8. Discharge-chamber performance of the LMT-20-I thruster in its ninth variation.

only over the upstream two-thirds of their length, as is done in the new thruster to avoid interference with the outer anode connector. Operation of the thruster with the alternative electromagnets was accompanied by a marked decrease in the level of discharge-chamber performance, although the shape of the magnetic field (measured by iron-filing plots) was modified almost imperceptibly. Six variations of the second stage configuration have not yet restored thruster performance to the level shown in Fig. 8.

## B. LIQUID MERCURY FEED SYSTEM

Assembly of the LMT-20-II feed system is now under way. To insure that no gases are trapped in the mercury feed lines, all elements of the feed system will be connected in their final configuration and pumped under high vacuum before vacuum-distilled mercury is introduced into the system. Although all of these elements will have been newly fabricated or assembled, prototype models of each of the components have been tested and shown to operate satisfactorily. The prototype LM cathode, designated K-51, was operated extensively during both phases of the current contract[5,6] and measurements of its specific thermal loading are presented in Section IV-C of this report. Development of single-capillary impedances was reported under the first phase of the contract,[6] and capillaries SC-3 and SC-4 which were tested at that time are currently in use as flow impedances for the liquid mercury flow bench and LM cathode K-51, respectively. Development of the liquid mercury flowmeter was described in Quarterly Progress Report No. 1 (Phase II) and satisfactory operation of both the electromagnetic pump and the high-voltage isolator is reported below.

### 1. Electromagnetic Pump

As reported in Quarterly Progress Report No. 1 (Phase II), replacement of the stainless steel electrodes with a dimensionally identical pair of molybdenum electrodes resulted in a marked decrease in power expended by the electromagnetic (EM) pump while maintaining the same pumping characteristics in terms of flow capacity and pressure change per ampere of electrical current. As before, the pump generates a pressure head of ±0.6 atm when driven at ±20 A. This power reduction was attributed to superior mercury wetting of the molybdenum surface which reduces the resistance across the pump to the value imposed by the electrical resistance of the mercury itself. During an 800 hour life test of the EM pump with molybdenum electrodes, a gradual increase occurred in the voltage drop across the pump until it had risen to over five times its initial value. Accompanying the voltage increase, small

bubbles of gas appeared on the surface of the glass tube which formed the mercury flow circuit. Since the entire flow system was enclosed within a vacuum environment, it was presumed that the source of the gas was from atmospheric elements dissolved within the liquid mercury itself. Even though the mercury had been triply distilled under vacuum prior to sale, sufficient time had elapsed for atmospheric gases to be absorbed by the mercury during storage.

During the last quarter, a second life test was performed which indicates that gas bubbles dissolved within the mercury were in fact the primary cause for the increase in internal resistance of the EM pump which was observed during the first life test. The same pump used during the first 800 hour life test was disassembled and the electrodes were cleaned and replaced. The glass tubulation forming the mercury flow circuit was modified so that mercury could be distilled and condensed into the flow system under a vacuum environment of $10^{-5}$ Torr. The pump was subsequently operated for 800 hours, with a total of $2.4 \times 10^6$ A-hours of mercury flow equivalent circulated through the pump, as in the previous test. During the entire test, the voltage drop across the pump increased only slightly from 0.076 V to 0.097 V at an electrical current flow of 20 A.

## 2. Hydrogen-Bubble High-Voltage Isolator

Satisfactory performance has been demonstrated by operation of the prototype model of the high-voltage (HV) isolator, which is shown in Fig. 9. This isolator employs an iron diffuser element to regulate the flow of hydrogen gas which enters the mercury flow stream as it passes through a section of insulated tube.[6,7] To initiate operation of the isolator assembly, the temperature of the diffuser element was adjusted to a value at which the hydrogen bubbles were injected into the mercury stream with a length of 1 cm. After 20 hours of operation overnight, the bubble length had increased to approximately 10 cm as a result of increased hydrogen flow rate caused by conditioning or flushing of the diffuser element. Following this initial start-up transient, the temperature of the diffuser element was lowered to a level at which bubbles of 1 cm length were again produced. After 80 hours of subsequent operation, with no further adjustments in the diffuser temperature, operating characteristics of the HV isolator were investigated as a function of the temperature of the diffuser element and the mercury flow rate.

The HV isolator was operated first at a bubble production rate of 4 bubbles/hour. At a mercury flow rate equivalent $I_a = 0.6$ A, a standby power level of 1.5 W combined with 2-min power pulses each quarter hour of 4.8 W was sufficient to inject hydrogen bubbles which are 1 cm long (see Fig. 10). The temperature of the diffuser element varied

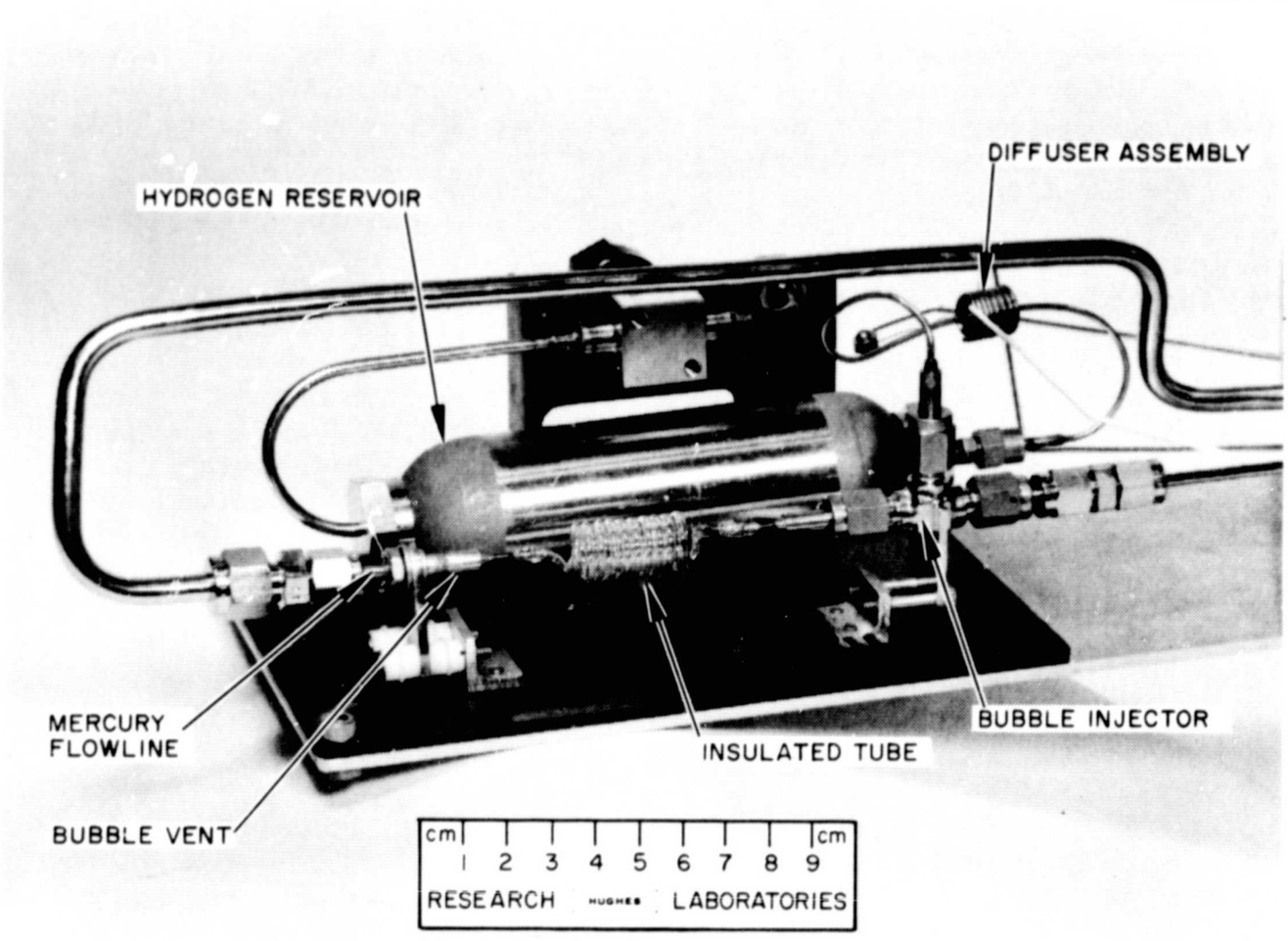


Fig. 9. Prototype model of the high-voltage isolator assembly.

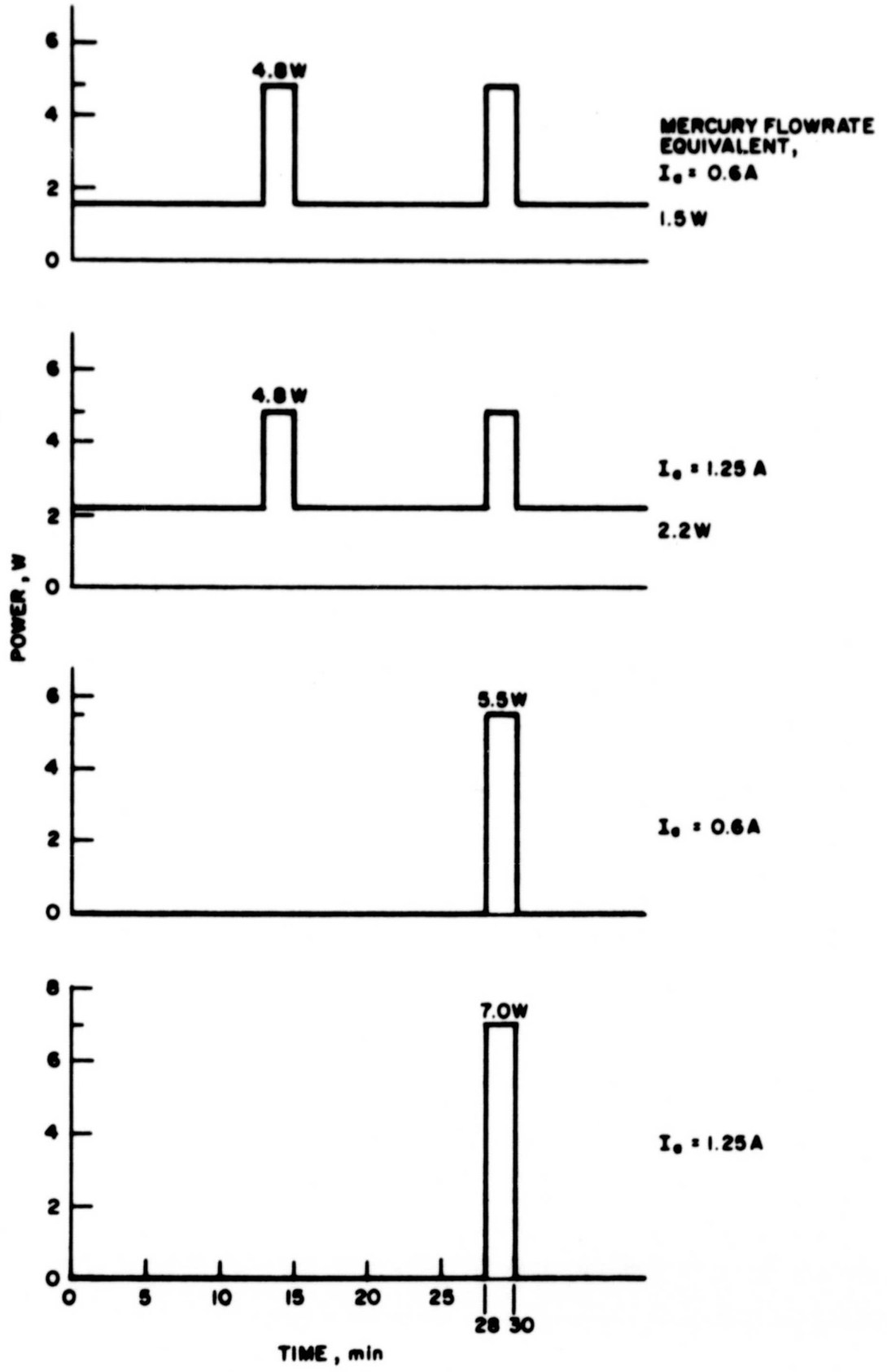


Fig. 10. Power levels required for production of 1 cm long hydrogen bubbles at various mercury flowrates.

between 315 and 390°C under the conditions of the test, which was conducted with an ambient background temperature of 30°C. At a mercury flow rate equivalent $I_a$ = 1.25 A, equivalent performance was achieved by raising the standby power level to a value of 2.2 W, while leaving the 2-min power pulses at a level of 4.8 W.* At this increased power level, the temperature of the diffuser element varied between 350 and 395°C.

In a second mode of operation, the production rate was reduced to 2 bubbles/hour and no standby power was employed. These simplifications were made possible by taking advantage of the long thermal response time of the diffuser assembly. To produce hydrogen bubbles which are 1 cm long, 2-min pulses of 5.5 W and 7.0 W were required for mercury flow rate equivalents $I_a$ = 0.6 A and 1.25 A, respectively. The required power levels resulted in a temperature variation of the diffuser element of from 150 to 295°C at $I_a$ = 0.6 A and from 160 to 320°C at $I_a$ = 1.25 A under the test conditions.

The HV isolator was operated continuously for 350 hours while its operating characteristics were determined. An additional 200 hours of running time has been accumulated in the second mode of operation (which requires no standby power) with high voltage (2 kV) applied. The effectiveness of the isolation was monitored with a strip-chart recorder, and no short-circuits were observed during this time.

The isolator has subsequently been turned off several times so that the transient operating characteristics during start-up could be observed. When the isolator is started (in the mode requiring no standby power), the diffuser element approaches its maximum operating temperature after the first power pulse, and a bubble is produced. The first bubble passes out of the injector region and into the insulated tube after a time of from 10 to 20 min, depending on the mercury flow rate. Operation proceeds normally thereafter.

*The required increase in standby power with increased flow rate was necessary with the prototype setup only, and will not be required for operation of the complete LMT-20-II mercury flow system. This increase compensates for the greater driving pressure at the isolator location, which is associated with increased flow rate and otherwise tends to reduce the bubble length. In the LMT-20-II system, all pressure variations are induced by means of the electromagnetic pump which is located downstream of the HV isolator.

The lightweight titanium hydrogen storage reservoir is completed and is presently being installed as part of the thruster feed system. The reservoir was pressure tested by a government approved testing laboratory (Wyle Testing Laboratory) at 1000 psia with no resultant leakage or deformation.

## C. LM CATHODE

A new, single-capillary, high-temperature LM cathode designated K-54 was constructed for use with the LMT-20-II thruster. As described in Quarterly Progress Report No. 1 (Phase II), its internal construction is essentially identical to that of LM cathode K-51, which was developed under the first phase of this contract.[6] During the last quarter of the current phase, the specific thermal loading $V_{K,th}$ of LM cathode K-51 was measured* as a function of the cathode body temperature $T_K$. As shown in Fig. 11, the specific thermal loading at 155°C is equal to 4 W/A, the value which is used in the thermal analysis presented in Section III of this report.

*$V_{K,th}$ is defined as the ratio of (thermal power $P_{K,th}$ received by the LM cathode from the discharge) to (electron current $I_K$ delivered by the LM cathode to the discharge): $V_{K,th} = \frac{P_{K,th}}{I_K}$.

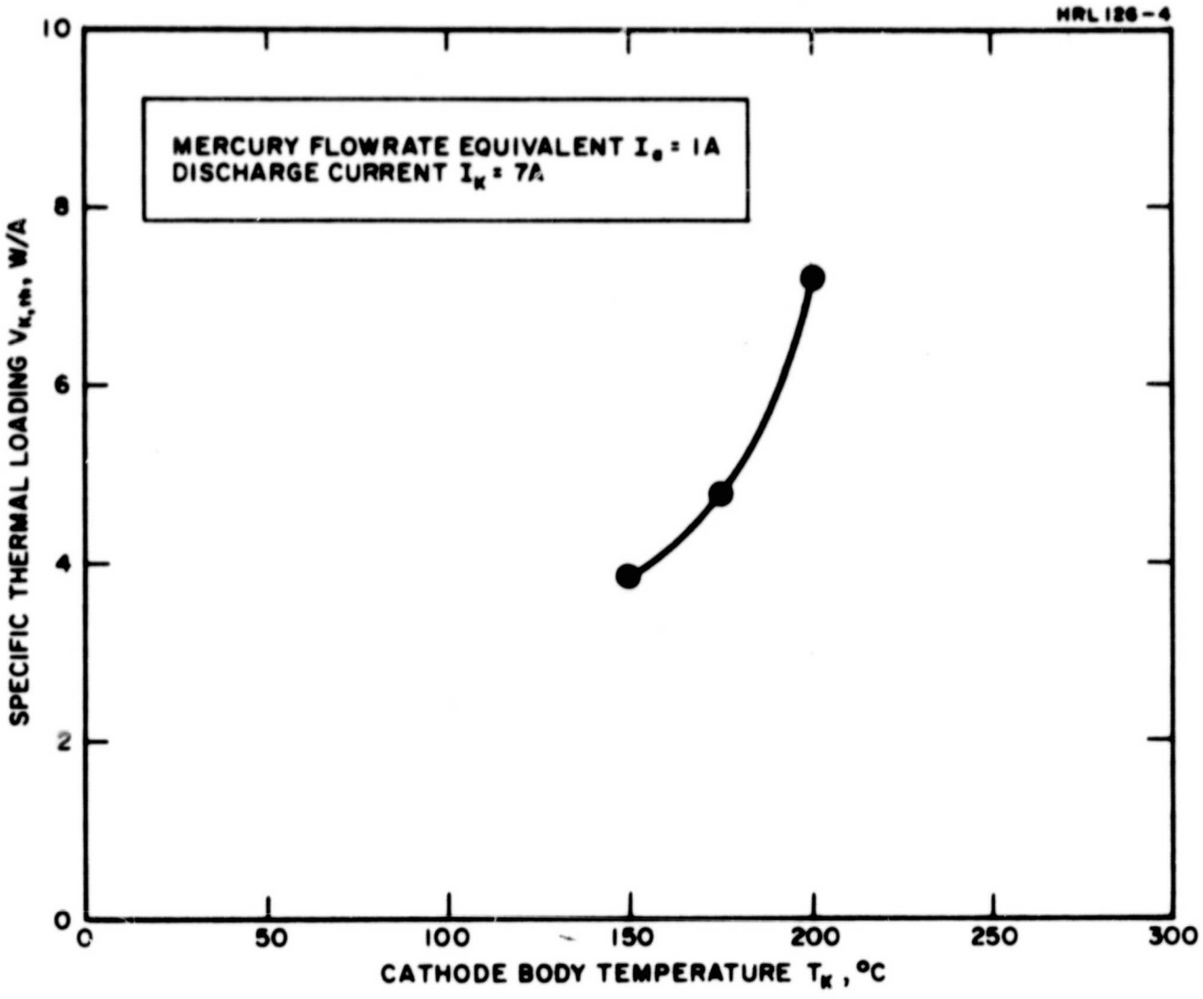


Fig. 11. Specific thermal loading $V_{K,th}$ as a function of the body temperature $T_K$ of LM cathode K-51.

# SECTION V

# CONCLUSIONS

The program to construct a 20 cm LM cathode thruster system (designated the LMT-20-II system) is nearing completion. Performance of the LMT-20-II thruster will be optimized for operation at beam currents $I_B$ = 0.5 to 1.0 A with a beam voltage $V_B \gtrsim 2$ kV. Prototype components of all elements of the thruster system have demonstrated satisfactory performance in operation under the current effort.

Accomplishments under the current phase of this contract include the following:

1. The experimental LMT-20-I thruster is being optimized for operation at a beam voltage $V_B$ = 2 kV with beam currents in the range $I_B$ = 0.5 to 1.0 A in order to predetermine optimization modifications which will be useful with the LMT-20-II thruster. The best performance to date has been achieved at a beam current $I_B$ = 950 mA with a total source energy per ion $V_S$ = 383 $\frac{eV^*}{ion}$ and a mass utilization efficiency $\eta_m$ = 88%.

2. The LMT-20-II thruster has been assembled and optimization testing has begun.

3. A prototype model of a liquid-mercury flowmeter has been tested and shows promise of a measurement accuracy of ±1%. The flowmeter will operate with a power expenditure of 1 W.

4. An electromagnetic pump using molybdenum electrodes has been operated stably for over 800 hours at a pressure rise of ±0.6 atm with a power expenditure of 2 W.

5. A high-voltage isolator has been developed and has been operated reliably and repeatably for over 500 hours. The average power expenditure can be as low as 0.4 W when it is operated in the pulsed-only heating mode.

*$V_S$ is the total source energy per ion, since no heater, vaporizer, or keeper power is required with the LM cathode.

6. The thermal profile of the LMT-30-I thruster has been calculated by analytical techniques and shown to agree with the experimentally measured profile. This correspondence confirms the validity of the analytical approach.

7. Thermal analysis indicates that the temperature of the LMT-20-II thruster will remain within acceptable limits when operated within the design current range. It has been concluded also that groups of thrusters operated in infinite planar clusters will achieve satisfactory thermal balance by self-radiation alone, so long as the separation between thrusters is at least equal to twice the thruster diameter.

# SECTION VI

## RECOMMENDATIONS AND FUTURE PLANS

During the next quarter, the program will continue along the following lines:

- The new LMT-20-II thruster will be tested and modified as required to optimize its performance for operation with beam currents in the range $I_B$ = 0.5 to 1.0 A. The LMT-20-I thruster will be available for concurrent operation to serve as a test-bed for proving out any major modifications of the discharge-chamber geometry before similar modifications are attempted in the LMT-20-II thruster.

- Thermal analysis will be undertaken to study the two cases of an infinite linear array of LMT-20-II thrusters with variable spacing between thrusters, and a peripheral array with variable spacing between thrusters.

- Assembly of the LMT-20-II feed system will be completed. With the new LM cathode K-54 attached, the feed system will be tested in vacuum to confirm the proper operation of each of the components (including LM cathode K-54) before it is integrated with the LMT-20-II thruster. The feed system will be filled with mercury by vacuum distillation, the mercury distillate being collected directly within the feed-system reservoir where it will be kept from contact with the atmosphere until it is consumed in the thruster discharge.

# SECTION VII

# NEW TECHNOLOGY

## A. FIRST QUARTER

During the first quarter of the current phase of this contract, an invention which is believed to be patentable was reduced to practice. Accordingly, the following patent disclosure was submitted to the Patent Department of the Hughes Aircraft Company.

PD 69419, Sensitive Liquid-Metal Flow Meter, by Julius Hyman, Jr.

The principles upon which this invention is based are reported to NASA on pp. 21-23 of the First Quarterly Report, 15 May 1968, covering Phase I of this contract. Further details concerning the operation of this device are contained on pp. 35-37 and in the Appendix of Quarterly Progress Report No. 1, 15 October 1969, covering Phase II of this contract.

## B. SECOND QUARTER

No reportable items of new technology were identified during the second quarter of the subject effort.

## REFERENCES

1. W. Knauer, "Power Efficiency Limits of Kaufman Thruster Discharges," to be presented at AIAA 8th Aerospace Sciences Meeting, New York, January 1970.

2. W.O. Eckhardt, K.W. Arnold, G. Hagen, J. Hyman, Jr., J.A. Snyder, and R.C. Knechtli, "High-Temperature Liquid-Mercury Cathodes for Ion Thrusters," Summary Report, Contract No. NASW-1404, Hughes Research Laboratories, July 1967.

3. W. Knauer, R.L. Poeschel, H.J. King, and J.W. Ward, "Discharge Chamber Studies for Mercury Bombardment Ion Thrusters," Final Report, Contract No. NAS 3-9703, Hughes Research Laboratories, September 1968.

4. W.L. Wolfe, Handbook of Military Infrared Technology (Office of Naval Research, Washington, D.C., 1965).

5. J. Hyman, Jr., J.R. Bayless, D.E. Schnelker, J.W. Ward, and R.L. Seliger, "LM Cathode Thruster System," Quarterly Progress Report No. 1, Phase II, Contract No. JPL 952131, Hughes Research Laboratories, 15 October 1969.

6. J. Hyman, Jr., W.O. Eckhardt, J.R. Bayless, J.A. Snyder, and J.W. Pfeifer, "High-Temperature LM Cathode Ion Thrusters," Final Report, Contract No. JPL 952131, Hughes Research Laboratories, 1969.

7. J.H. Molitor, H.J. King, and S. Kami, "A Study of Liquid Mercury Isolator Development," Final Report, Contract No. NAS 7-539, Hughes Research Laboratories, September 1969.